

Use of a reduced-gravity model to evaluate present and past primary productivity in the tropical open ocean

*Itsuki C. Handoh*¹ and *Grant R. Bigg*

School of Environmental Sciences, University of East Anglia, Norwich, United Kingdom

Masamichi Inoue

Coastal Studies Institute and Department of Oceanography and Coastal Sciences, Louisiana State University, Louisiana

Abstract

Upwelling predicted by a reduced-gravity model is compared with remotely sensed primary productivity data through the tropical Atlantic and Pacific. The model upper layer thickness, an indicator of vertical motion, is correlated with primary productivity. We suggest that the Atlantic basin is more efficient than the Pacific in its production for the same degree of upwelling. This is a characteristic of the tropical Pacific ecological provinces being featured by low salinity in the western tropics and high nutrient, but low chlorophyll in the eastern equatorial region. A comprehensive relationship between model upper layer thickness and primary productivity is established through the tropical basins, with emphasis on the equatorial strip. Our work has implications for the application of reduced-gravity models to estimate productivity in palaeocean studies.

Variability in the tropical oceanic boundary layer is of interest from the climatic perspective, but is also of biological importance because of the oceanic productivity sustained within this relatively thin layer. Wind-induced upwelling (downwelling) plays a vitally important role in reducing (enhancing) the heat storage of the mixed layer above the thermocline. Ecologically, enhancement (suppression) of nutrient supplies associated with entrainment (detrainment) across the thermocline results in rich (poor) oceanic productivity during the time of upwelling (downwelling) (Luther et al. 1990). Thus regions where strong upwelling is seen include some of the major fisheries of the world. These effects are tied together in, for example, the El Niño events in the tropical Pacific. Upwelling studies are also of economic importance because of the links between the siting of fossil fuel resources (such as oil and natural gas) and oceanic productivity of the geologic past (Parrish and Curtis 1982; Handoh et al 1999). Quantification of upwelling is, therefore, of interest to scientists in various fields.

Upwelling and downwelling can be predicted and quantified by several types of ocean models that incorporate upper ocean dynamics. A reduced-gravity 1.5 layer numerical model originally developed by O'Brien et al. (1978) is frequently used in the tropics. The model formulation reduces

the ocean to two homogeneous layers, with most of the essential physics within the upper layer being retained. For example, Rossby wave propagation in the upper ocean, being one of the key mechanisms to explain enhanced primary production through pumping nutrients to ocean surface (Uz et al. 2001), is clearly identified in the model. This model is capable of explaining intraannual and interannual variability in the tropical upper layers, and it has been extensively tested in the modern oceans (e.g., Busalacchi and Blanc 1989; Inoue and Welsh 1993). Past El Niño events have been successfully simulated by this model (Inoue and O'Brien 1986; Bigg and Inoue 1992).

The reduced-gravity model used here is also applicable to palaeocean studies (Luther et al. 1990; Handoh et al. 1999). Climatological upwelling intensity, in terms of the model upper layer thickness, is consistent with foraminiferal records (Luther et al. 1990) and organic-rich sedimentary deposits (Handoh et al. 1999). Difficulties in appropriately constraining palaeothermohaline processes and palaeobathymetry are avoided by employing this type of model. Because of the many unknown factors in such a study, a reduced-gravity model with simple open boundary conditions such as those of Camerlengo and O'Brien (1980) may be preferable to general circulation models for basin-scale or regional studies of palaeocean circulation forced by a palaeoatmospheric reconstruction. Despite this potential use of reduced-gravity models, however, their ability to quantitatively assess oceanic productivity via predicted upwelling intensity has not yet been reported.

In studying modern-day ocean productivity, an interesting issue stems from the relationship between ecological oceanographic biomes, productivity, and wind-driven upwelling. Longhurst et al. (1995) made an ecological geography, based on detailed reviews of ecological oceanography and Coastal Zone Color Scanner (CZCS)-derived phytoplankton pigment concentrations. The tropical open oceans (roughly 30°S–30°N) are classified as the trade biome, where the mixed layer depth is forced by geostrophic adjustment on ocean

¹Corresponding author (i.handoh@uea.ac.uk).

Acknowledgements

This work was supported in part by NATO grant CRG-972147 and the School of Environmental Sciences of the University of East Anglia. We thank two anonymous reviewers for very constructive comments that improved this paper. Dorota Kolber at the Institute of Marine and Coastal Sciences of the State University of New Jersey, Rutgers, graciously supplied the VGPM primary productivity data. I.C.H. also thanks Dr. Susan Welsh of the Coastal Studies Institute at Louisiana State University for computing support during his visit to LSU, and ENV colleagues in biogeochemistry for their help.

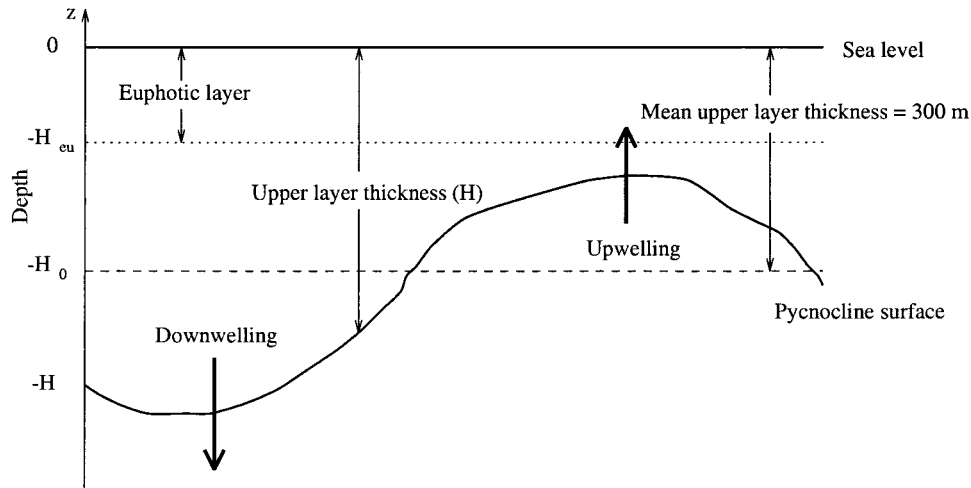


Fig. 1. Schematic diagram of the two-layer structure of the model ocean. Upwelling (downwelling) occurs where H is smaller (greater) than H_0 .

basin scale to remote forcing of the winds. Wind-driven upwelling provides the mixed layer with nutrient-rich water. However, the eastern equatorial Pacific is a high-nutrient, low-chlorophyll (HNLC) region (Price et al. 1994; Longhurst 1998). Vast amounts of nutrients can be supplied by wind-driven equatorial upwelling, but iron availability in this region constrains its productivity (Behrenfeld and Kolber 1999). It is also noteworthy that grazing is the proximate control on the standing crop of phytoplankton, while the micronutrient, iron could ultimately regulate productivity (Cullen et al. 1992). Macronutrient injection associated with upwelling is still an integral control of oceanic productivity (Herzfeld 1992), regardless of the constraints due to iron availability and grazing. The western tropical Pacific is also a unique province in the trade biome, due to the heavy rainfall sustaining a shallow halocline (“barrier layer”) over the region (Lukas and Lindstrom 1991). By contrast, the trade biome found in the tropical Atlantic does not exhibit such characteristics. This suggests that the tropical Pacific has the potential to show a clear difference in the relationship between upwelling and productivity from the tropical Atlantic.

In this paper, using a reduced-gravity upper ocean model and remotely sensed primary productivity data, we assess upwelling and downwelling in the tropical Atlantic and Pacific basins. We begin with a description of the reduced-gravity upper ocean model, followed by a brief investigation into the upwelling and downwelling regions predicted by the model. Subsequently, the one-dimensional nutrient balance of the upper ocean is considered so as to establish the relationship between displacement of the model upper layer thickness and primary productivity. Upwelling and downwelling in the tropics are then classified ecologically by a quantitative comparison between upper layer thickness and the primary productivity. We will discuss the extent to which both wind-driven upwelling and vertical eddy diffusion of nutrient sustain primary productivity. The major differences in productivity between the two basins are explained by the geographical distribution of aeolian iron fluxes over the tropics (Gao et al. 2000). This quantitative comparison between

the model upwelling and primary productivity gives us confidence in the palaeointerpretation of the model results of Luther et al. (1990) and Handoh et al. (1999).

The model ocean

Model description—The reduced-gravity ocean consists of a single active layer, of variable thickness and depth-integrated velocities, above a quiescent abyss (Fig. 1). A single baroclinic wave mode is included in this type of model; either the first or second is usually taken. For our study we have taken the nonlinear, spherical reduced-gravity formulation in which the open boundary conditions (OBCs) of Camerlengo and O’Brien (1980) and Kelvin wave propagation scheme of Inoue and Welsh (1993) are implemented.

We define variables λ , φ , U , V , and H to represent longitude, latitude, vertically integrated zonal velocity, vertically integrated meridional velocity, and upper layer thickness (or pycnocline depth), respectively. Ω is the angular velocity of the earth, and R is the radius of the earth. The reduced gravity is $g' = g(\rho_2 - \rho_1)\rho_2^{-1}$, where ρ_1 , ρ_2 , and g denote the density of the upper layer, of the lower layer, and the gravitational acceleration respectively. The kinematic eddy viscosity, A_H is taken as constant. The model is forced by the wind stress vector $\vec{\tau} = (\tau_\lambda, \tau_\varphi)$. We will use the climatological monthly mean wind stress of Hellerman and Rosenstein (1983), interpolated onto the ocean model grid.

Using the so-called rigid-lid and hydrostatic approximation, the full equations of motion in the spherical coordinate system are

$$\frac{DU}{Dt} - 2\Omega \sin \varphi V = -\frac{g'}{2R \cos \varphi} \frac{\partial H^2}{\partial \lambda} + \frac{\tau_\lambda}{\rho_1} + A_H \nabla^2 U \quad (1)$$

$$\frac{DV}{Dt} + 2\Omega \sin \varphi U = -\frac{g'}{2R} \frac{\partial H^2}{\partial \varphi} + \frac{\tau_\varphi}{\rho_1} + A_H \nabla^2 V \quad (2)$$

$$\frac{\partial H}{\partial t} + \frac{1}{R \cos \varphi} \left(\frac{\partial U}{\partial \lambda} + \frac{\partial}{\partial \varphi} (V \cos \varphi) \right) = \frac{(H_{\min} - H)^2}{T_E H_{\min}} \quad (3)$$

Table 1. Governing parameters. See also Inoue and Welsh (1993).

Parameter	Description	Value
Δt	Time step	20 min
$\Delta \lambda$	Zonal resolution	0.25°
$\Delta \varphi$	Meridional resolution	0.25°
A_H	Horizontal eddy viscosity	750 m ² s ⁻¹
ρ_1	Upper layer density	1026 kg m ⁻³
H_0	Initial upper layer thickness	300 m
H_{\min}	H below which entrainment process occurs	60 m
T_e	Time constant for entrainment rate	1 h

where Lagrangian and Laplacian operators on any variable α are defined respectively by

$$\frac{D\alpha}{Dt} \equiv \frac{1}{R \cos \varphi} \frac{\partial}{\partial \lambda} \left(\frac{U\alpha}{H} \right) + \frac{1}{R} \frac{\partial}{\partial \varphi} \left(\frac{V\alpha}{H} \right) \quad (4)$$

$$\nabla^2 \alpha \equiv \frac{1}{R^2 \cos^2 \varphi} \frac{\partial^2 \alpha}{\partial \lambda^2} + \frac{1}{R^2 \cos \varphi} \frac{\partial}{\partial \varphi} \left(\cos \varphi \frac{\partial \alpha}{\partial \varphi} \right) \quad (5)$$

The values for each parameter are summarized in Table 1. The right-hand side of Eq. 3 is the model entrainment rate (see McCreary and Kundu 1988). This is nonzero only when the model upper layer thickness (H) reduces below the preset value, H_{\min} . T_e is the time constant for entrainment rate.

The upper layer thickness (H) represents, by definition, a pycnocline depth, comparable to the 1,028 kg m⁻³ isopycnal (to be shown later) or the 14°C isothermal depth (Inoue and Welsh 1993). This generally locates well below the seasonal mixed layer. Owing to the model's physics, it does not provide an explicit vertical velocity. However, the displacement of H relative to the model's initial H (H_0), ΔH ($=H - H_0$), is a well-established measure of upwelling ($\Delta H < 0$) and downwelling ($\Delta H > 0$) (e.g., O'Brien et al. 1978; Luther et al., 1990).

The tropical Atlantic—Figure 2A shows the Atlantic ocean model domain extending meridionally from 30°S to 30°N and zonally from 100°W to 20°E. The model land boundaries were taken along the 300-m isobath (Naval Oceanographic Office 1983). Real coastlines are drawn in Fig. 2B. We have used a g' of 0.025 m s⁻², the other governing parameters of the model are identical to those in Inoue and Welsh (1993). The northern and southern boundaries are open. The model was run with the annual cycle in monthly wind forcing and settled down to a repeatable cycle within 10 yr.

Results show the output for the 11th year of the simulation. The pattern of the model's annual mean upper layer thickness, shown in Fig. 2A, is in good agreement with the results of Busalacchi and Blanc (1989). The tropical half of each subtropical gyre is clearly illustrated. Steep gradients of H along the western boundaries are indicative of the western boundary currents, the Gulf Stream, and Brazil Current in the northern and southern hemispheres, respectively. The equatorial and eastern regions are covered with an extensive upwelling cell. This is consistent with an annual mean up-

welling over 15°S–15°N, predicted by a quasi-geostrophic model (Wunsch 1984). Northeastern and southeastern maxima in the upwelling region occur in the intense coastal upwelling area including the Canary and Benguela Currents, respectively. Note that model entrainment did not occur in the tropical Atlantic basin.

The tropical Pacific—We extended the results of Inoue and Welsh (1993). The governing parameters of our Pacific model are the same as those in Inoue and Welsh (1993), but the model domain was extended to cover 46°S to 72°N and 100°E to 60°W (Fig. 3A) in comparison to 30°S to 30°N in Inoue and Welsh (1993). Note that there is no Bering Strait connecting to the Arctic, as the model land boundaries were taken along the 300-m isobath, as described in the last subsection. Thus, the open boundary conditions are applied only for the southern and southwestern boundaries. The relaxation method used in Inoue and Welsh (1993) for the southwest corner, in the eastern Indian Ocean, is also employed in this study. The model was run with the annual cycle in monthly wind forcing and settled down to a repeatable cycle within 23 yr.

Results show the output for the 26th year of the simulation. An extremely strong upwelling ($H < 60$ m) occurred in the northern subpolar gyre, which resulted in an active model entrainment. However, this did not affect the patterns of the model's annual mean upper layer thickness over the tropical basin, these being very comparable with the results of Inoue and Welsh (1993). This suggests that the choice of meridional extent of the model domain does not alter the magnitudes of upwelling and downwelling in the tropics. The western boundary currents, Oyashio, Kuroshio, and East Australian Current, are clearly produced, and intense upwelling regions over the tropical to subtropical latitudes are present in the California Current, equatorial cold tongue, and along the South American coast. It is noteworthy that here the reduced-gravity model has successfully simulated major features of the ocean circulation over the pan-Pacific basin rather than only its tropics.

Nutrient balance in the “nitraclinic” upper ocean

Figure 4A,B shows the annual mean meridional vertical cross-section of model H , isopycnal surfaces, and nitrate distribution of the central tropical Atlantic (25.5°W) and central tropical Pacific (150°W), respectively. Total nitrate distribution is a proxy of nutrient content. Model H is comparable with the 1,028 kg m⁻³ isopycnal depth for both tropical basins. The model pycnocline generally intersects with isopleths of nutrient, which we call the nitraclinic.

Consider a one-dimensional balance of the total inorganic nutrient content, N (g m⁻³) in the reduced-gravity upper ocean. The time evolution of N is controlled by biological consumption, vertical momentum, and eddy diffusion. The governing equation is

$$\frac{\partial N}{\partial t} + \frac{\partial}{\partial z} (wN) = \frac{\partial}{\partial z} \left(K \frac{\partial N}{\partial z} \right) - \eta N \quad (6)$$

where w (m s⁻¹) and K (m² s⁻¹) are the vertical velocity and

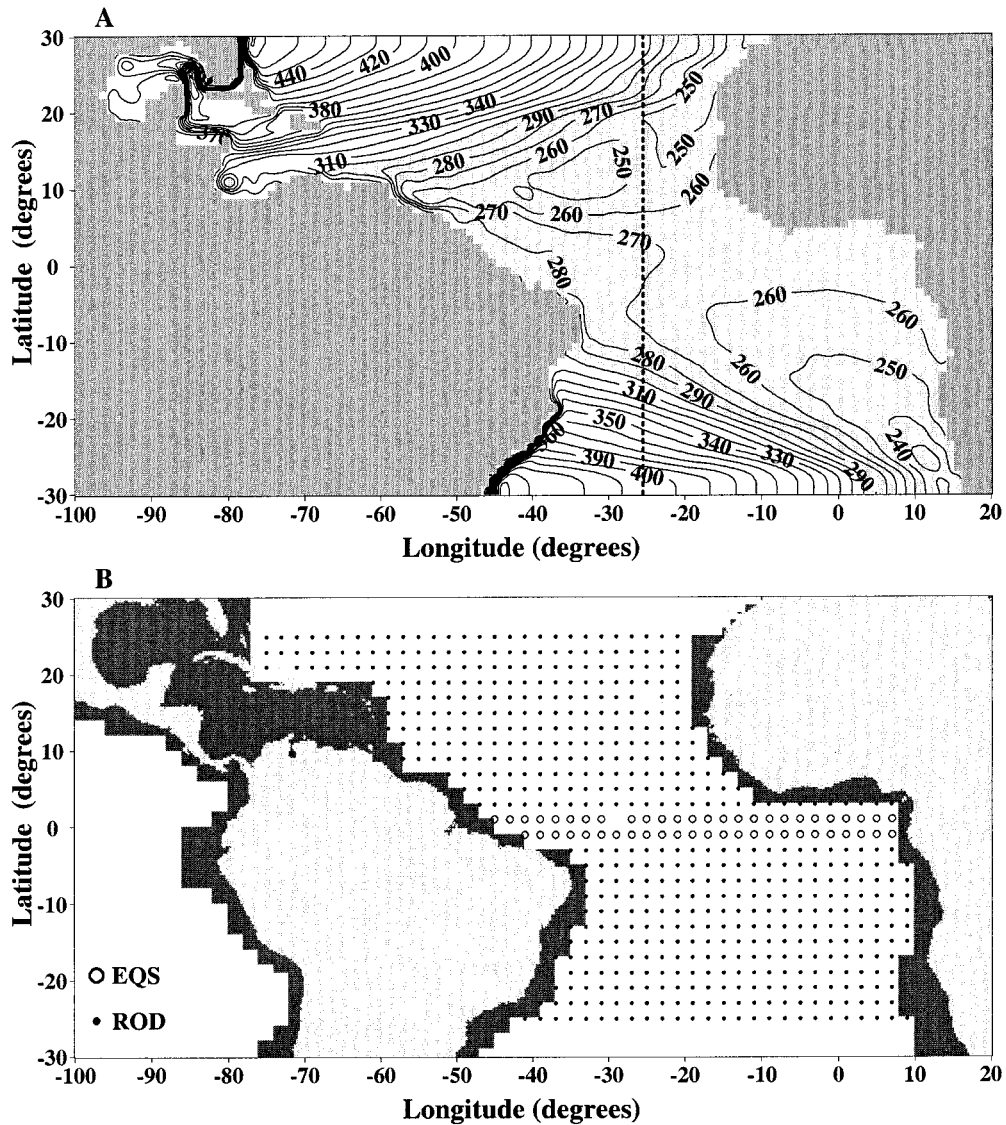


Fig. 2. (A) Annual mean upper layer thickness (in meters) from the 11th year output of the Atlantic model. The contour interval is 10 m. Upwelling region ($H < 300$ m) is shaded. Solid-dotted straight line is the position of the vertical cross-section in Fig. 4A. (B) Continents (light tone) and Longhurst et al.'s (1995) Coastal and Caribbean Provinces (dark tone) in the tropical Atlantic. Samples used in the regression analysis between H and primary productivity (PP) are denoted by open circles and dots for equatorial strip (EQS) and rest of domain (ROD), respectively. A very few points of anomalously high primary productivity ($>1,000$ g C m $^{-2}$ yr $^{-1}$) in the open ocean are ignored, as these are presumably associated with very local coastal upwelling around the small islands.

eddy-diffusion coefficient, respectively, and η is the time constant of biological nutrient consumption in s $^{-1}$. The vertical coordinate is z . Vertically integrated ηN is equal to the new production of the layer (NP). Note that $NP \equiv PP - RP$ where PP and RP denote the total production and regenerated production, respectively.

Assuming a steady state and rigid-lid boundary condition, vertically integrating Eq. 6 from the model upper layer depth (an isopycnal depth below the euphotic zone), $-H$, to the sea surface (see Fig. 1), we define new primary production in g m $^{-2}$ s $^{-1}$ as

$$NP \equiv \int_{-H}^0 \eta N dz = (wN)|_{-H} - \left(K \frac{\partial N}{\partial z} \right) \Big|_{-H} \quad (7)$$

where the first and second terms of the right-hand side in Eq. 2 are vertical momentum flux of nutrient associated with upwelling/downwelling, and eddy diffusion of nutrient at the model pycnocline depth, $-H$, respectively. Note that in Eq. 7 H can be replaced by H_{eu} , since much of the primary production occurs in the euphotic layer.

Now we parameterize the momentum flux of nutrient, wN . In the reduced-gravity model, the pycnocline displacement,

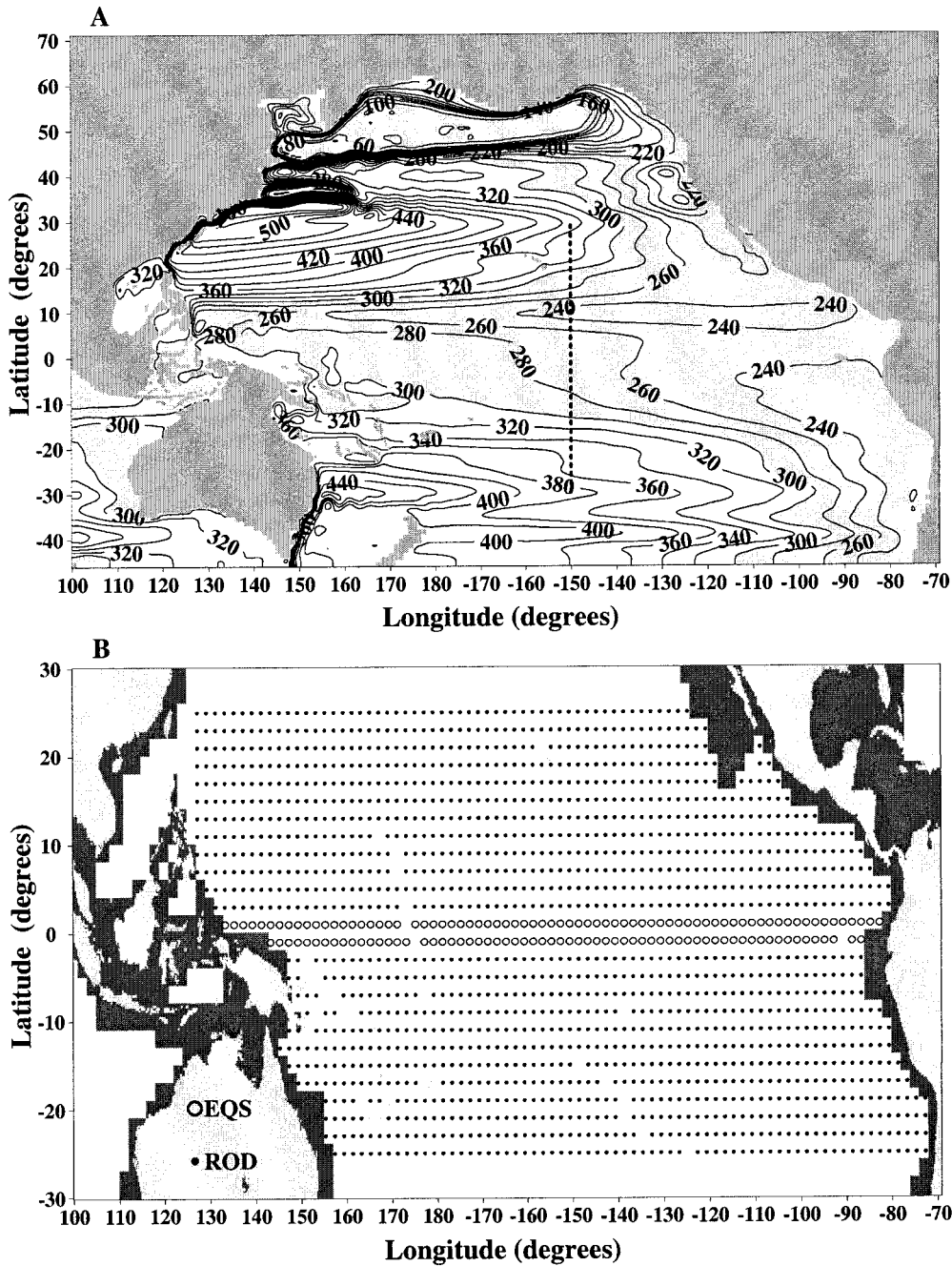


Fig. 3. (A) Same as Fig. 2A, but from the 26th year output of the Pacific model. The contour interval is 20 m. Solid-dotted straight line is the position of the vertical cross-section in Fig. 4B. (B) Same as Fig. 2B, but for the tropical Pacific.

ΔH , is indicative of w , and if w is linearly proportional to this,

$$w \propto -\Delta H \begin{cases} > 0 & \text{(Upwelling)} \\ < 0 & \text{(Downwelling)} \end{cases} \quad (8)$$

N at the pycnocline interface generally increases with decrease of ΔH , so $N \propto -\Delta H$ (see Fig. 4). This is the characteristic of the nitraclinic tropical ocean. Comparing N in the water column between upwelling and downwelling re-

gions shows that in the latter N is much lower than in the former (Fig. 4A,B). Hence, for convenience, we ignore the nutrient loss from the water column associated with downwelling, regardless of the magnitude of w . Thus the form of the vertical momentum of nutrient can be parameterized

$$(wN)|_{-H} = \begin{cases} q(\Delta H)^2 & (H_0 > H) \\ 0 & (H_0 \leq H) \end{cases} \quad (9)$$

where q is a constant. For the diffusion term, let K be a

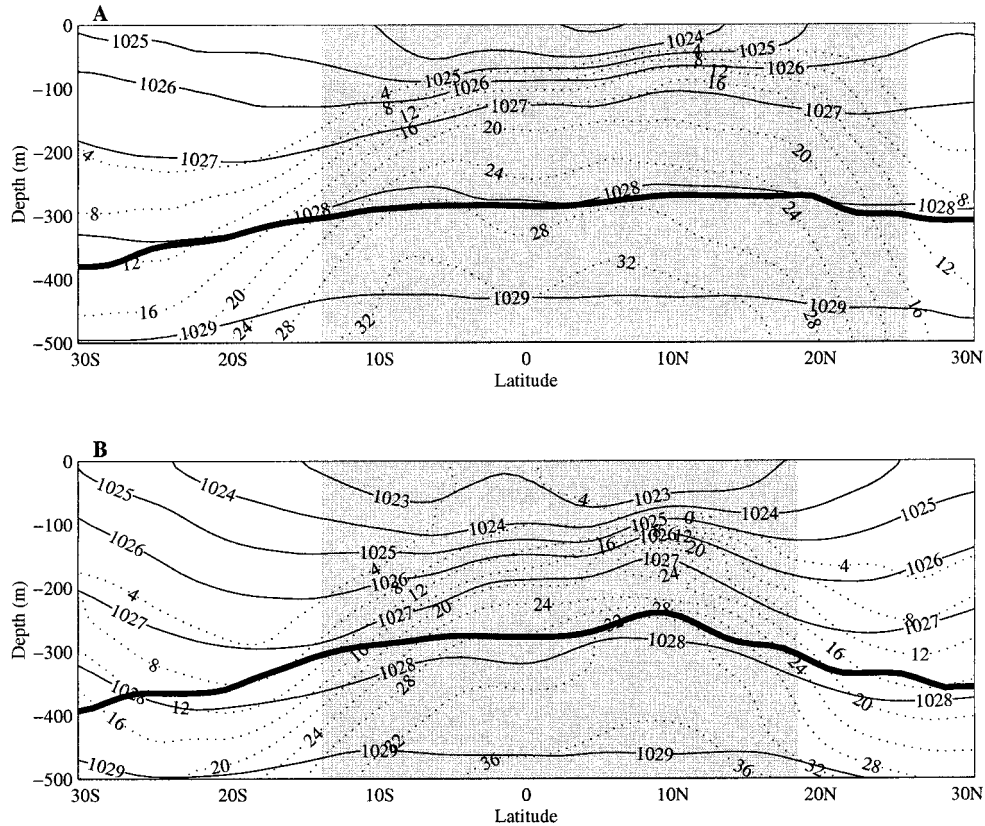


Fig. 4. (A) Vertical cross-section along 25.5°W of the central tropical Atlantic. Isopycnal lines (in kg m^{-3}) and isopleths of nitrate (in $\mu\text{mol L}^{-1}$) are contoured by solid and dotted lines, with contour intervals of 1 kg m^{-3} and $4 \mu\text{mol L}^{-1}$, respectively. Data are from the annual mean climatology of Levitus and Boyer (1994). Thick line represents the model upper layer thickness (H). Upwelling area, predicted by the ocean model is shaded. See also Fig. 2A. (B) Same as A, but along 150°W of the central tropical Pacific. See also Fig. 3A.

constant (K typically ranges from 10^{-6} to $10^{-5} \text{ m}^2 \text{ s}^{-1}$). Note that the term is always positive, since the vertical gradient of nutrient across the pycnocline interface is negative (see Fig. 4). We define a minimum productivity, PP_0 , as the sum-

Table 2. Summary of regression analysis. Abbreviations are labeled: EQS, equatorial strip; ROD, rest of domain. South and North denote southern and northern hemispheric half of the ROD, respectively. Variables are the number of samples (n) in the upwelling region (tropical basin), the 95% confidence interval for the regression coefficients (PP_0 and k), and variance explained by the regression curves ($V = 100 \times r^2\%$). The regression analysis was conducted for samples in the upwelling region. See the main text.

	n	$\ln PP_0$ ($\text{g C m}^{-2} \text{ yr}^{-1}$)	k (10^{-4} m^{-2})	V (%)
Atlantic				
EQS	51 (51)	4.06 ± 0.11	8.86 ± 1.07	84.2
ROD	387 (545)	4.34 ± 0.07	3.11 ± 0.42	36.0
South	200	4.25 ± 0.11	3.49 ± 0.59	40.7
North	187	4.44 ± 0.10	2.73 ± 0.59	30.8
Pacific				
EQS	123 (136)	4.45 ± 0.04	1.76 ± 0.20	70.6
ROD	966 (1566)	4.22 ± 0.01	1.26 ± 0.09	42.3
South	446	4.30 ± 0.02	1.42 ± 0.09	69.6
North	520	4.16 ± 0.04	1.04 ± 0.15	27.6

of a new production sustained by the upward vertical diffusion of nutrient (NP_0) and regenerated production:

$$\left(-K \frac{\partial N}{\partial z}\right) \Big|_{-H} + RP = NP_0 + RP = PP_0 \quad (10)$$

In order to clarify the dimension of the right-hand side of Eq. 9, let $q = PP_0 k$. We then obtain from Eq. 7

$$PP = NP + RP = PP_0 [1 + k(\Delta H)^2 \Theta(H_0 - H)] \quad (11)$$

where k (in m^{-2}) is arbitrarily chosen to satisfy $q = PP_0 k$ and Θ is the unit step function. Since the dimensionless term $k(\Delta H)^2 \Theta(H_0 - H) < 1$ [note that the magnitudes of k and $(\Delta H)^2$ are 10^{-4} m^{-2} and 10^3 m^2 , respectively; see also Table 2], Eq. 11 can be rewritten as

$$PP \approx PP_0 e^{k(\Delta H)^2 \Theta(H_0 - H)} \quad (12)$$

Note that RP in the real ocean varies with the strength of upwelling, but Eq. 12 allows us to directly estimate the total primary productivity regardless of the nutrient origin.

Estimate of primary productivity

The Coastal Zone Color Scanner (CZCS) observed the phytoplankton pigment concentration (PPC) over the globe from November 1978 to June 1986. Longhurst et al. (1995)

used the PPC data to estimate global primary productivity as well as to partition the ocean into 57 biogeochemical provinces. The Sea-Viewing Wide Field-of-view Sensor (SeaWiFS), launched in September 1997, has a better spatial coverage in PPC data than the CZCS. Noting, however, that there was the most significant El Niño of 1997–1998 during the period of temporal coverage, it seems that SeaWiFS-derived PPC is still not appropriate for calculating the climatology.

We therefore employ the estimate of primary productivity (PP in $\text{g C m}^{-2} \text{ yr}^{-1}$) by the Vertically Generalized Production Model (VGPM; Behrenfeld and Falkowski 1997a,b), converted from the CZCS-derived PPC (mg m^{-3}) of November 1978–October 1981. The annual averaged PP over the available period (in which there was no significant El Niño and Atlantic warm event) is compared here with the annual mean climatology of the model H . Primary productivity in the tropics is less seasonally variable than in the middle and high latitudes, and this simple approach should be robust for palaeocean studies. It is stressed that the CZCS can observe only the net PPC through ecological interaction among nutrients, phytoplankton, and zooplankton, which is sustained by dynamical backgrounds. However, the VGPM result was well validated against observational datasets (Behrenfeld and Falkowski 1997a). In contrast, our ocean model can only estimate a proxy for nutrient supply due to upwelling. Any thermodynamical and biogeochemical backgrounds cannot be represented in the model. On the global scale, aeolian iron fluxes seem to sustain part of the primary productivity (Longhurst 1998; Gao et al. 2000). The distribution of such fluxes could be one of the major limiting factors for marine primary productivity. It should also be stressed that riverine inputs of nutrients are very important to sustain coastal productivity, such as in the Amazon delta (Müller-Karger et al. 1988; Bonilla et al. 1993). None of these biogeochemical factors is accounted for in the reduced-gravity model. Therefore the model's ability to assess primary productivity is necessarily limited. Nevertheless, our study will show the degree to which model-derived upwelling can explain ocean productivity.

Comparison between model-predicted upwelling and primary productivity

Procedure—In this paper we are concerned with climatological annual mean ocean productivity associated with upwelling in the tropics, and hence we focus on the region extending from 25°S to 25°N. For the Pacific model our study will ignore the Indian Ocean and the Indonesian region connecting the Pacific and Indian Oceans in the southwestern corner of the model domain (Fig. 3). This provides a better interbasin comparison of the Atlantic and Pacific. We also exclude coastal provinces of Longhurst's ecological classification because of the accentuation of primary productivity by nutrients of nonmarine origin (Müller-Karger et al. 1988; Bonilla et al. 1993), and the Caribbean province because a significant part of it is affected by coastal processes. These provinces are depicted in Figs. 2B and 3B for the Atlantic and Pacific, respectively. The VGPM shows

anomalously high primary productivity ($>1,000 \text{ g C m}^{-2} \text{ yr}^{-1}$) in a few areas of the open ocean. This may be due to very local coastal upwelling around small islands (see Figs. 2B and 3B). These extreme regions are also ignored.

Comparison—Scatter plots of the upper layer thickness (H) versus primary productivity (PP) for the tropical Atlantic and Pacific are shown in Fig. 5A,B, respectively. Grid points at a resolution of $2^\circ \times 2^\circ$ are plotted (see Figs. 2B and 3B for parts included). In the light of tropical ocean dynamics, we can classify the data into two distinct categories (see also Table 2):

1. An equatorial strip, which has the width of the equatorial Rossby radius of deformation (EQS).
2. The rest of the domain (ROD).

We determined the regression coefficients PP_0 and k from Eq. 12. It is important to note that for estimating the regression coefficients we ignore PP and H in the downwelling because $(\Delta H)^2$ is always zero when $H > H_0$. This approach, however, has little impact on the estimates of PP_0 and k .

In downwelling regions ($H > H_0$ in Fig. 5A,B), the productivity is nearly constant regardless of the strength of the downwelling. This is likely to be attributable to a weak upward nutrient diffusion through the thermocline (PP_0), as is consistent with our simple model in Eq. 10. This constant, PP_0 in ROD, is slightly larger in the Atlantic than in the Pacific (Table 2). This suggests that the background productivity in the Atlantic is slightly, but not significantly, higher than the Pacific. Eddy-induced upwelling associated with internal Rossby wave propagation can lead to the production above PP_0 in the general downwelling of the subtropical gyres (Fig. 5A,B) (Uz et al. 2001).

In all the upwelling regions ($H < H_0$ in Fig. 5A,B), in contrast, positive correlations between H ($= H_0 + \Delta H$) and PP are found. Another regression constant, k , is indicative of the effectiveness of production due to upwelling. The steep increase of productivity with upwelling is most distinct in the equatorial Atlantic ($r = 0.92, p < 0.05$). This indicates that productivity in the Pacific is rather less sensitive to upwelling, due to the dynamical and biogeochemical backgrounds of the two basins. We will discuss this later.

Figure 5A shows the two regression curves for the Atlantic, one for the EQS and the other for the ROD. The steeper curve shows the effectiveness of the production occurring within the equatorial strip. Regression analysis gives the 95% confidence limits of the regression coefficients, $k = 8.86 \pm 1.07 \times 10^{-4} \text{ m}^{-2}$ and $\ln PP_0 = 4.06 \pm 0.11$ (equivalent to $PP_0 = 51.9\text{--}65.3 \text{ g C m}^{-2} \text{ yr}^{-1}$), the latter being similar to the minimum productivity in the subtropical gyres of the Atlantic ($58.5 \text{ g C m}^{-2} \text{ yr}^{-1}$). Much of the subtropical gyres exhibit $PP < 100 \text{ g C m}^{-2} \text{ yr}^{-1}$. In fact, regression analysis for ROD shows $PP_0 = 71.7\text{--}82.9 \text{ g C m}^{-2} \text{ yr}^{-1}$ and $k = 3.11 \pm 0.42 \times 10^{-4} \text{ m}^{-2}$ ($r = 0.60, p < 0.05$).

Turning to the tropical Pacific, a similar trend to the tropical Atlantic is seen for the gentle curve representing the ROD ($r = 0.65, p < 0.05$), although both k and PP_0 are smaller ($k = 1.26 \pm 0.09 \times 10^{-4} \text{ m}^{-2}$, $PP_0 = 66.2\text{--}69.4 \text{ g C m}^{-2} \text{ yr}^{-1}$) than those in the Atlantic ROD. However, the equatorial regime (EQS) in the Pacific ($r = 0.84, p < 0.05$) is not as clear as that in the Atlantic. Table 2 shows a slightly

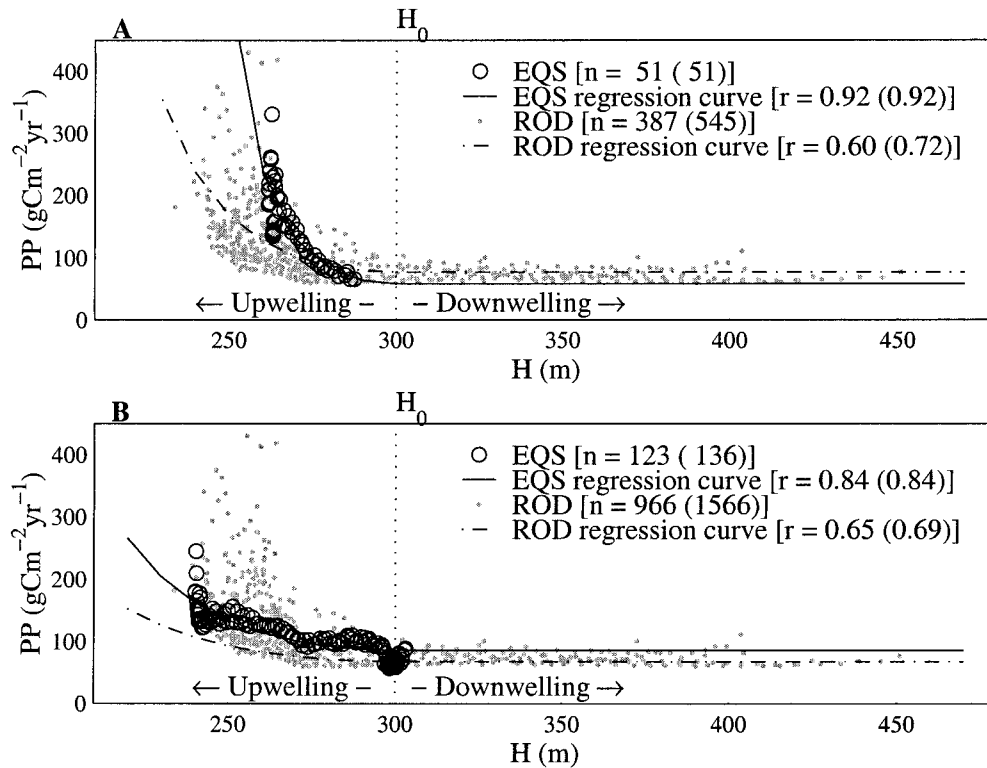


Fig. 5. Scatter plots of the model upper layer thickness in meters (H) versus remotely sensed primary productivity in $\text{g C m}^{-2} \text{ yr}^{-1}$ (PP). Curve-fittings are based on Eq. 12, with constants k and PP_0 , but only the upwelling region ($H < 300$ m) is considered for the regression analysis. Two numbers of samples (n) are shown; the numbers of samples in upwelling region and tropical basin, the latter being in brackets. Corresponding correlation coefficients (r) are also shown. (A) the tropical Atlantic and (B) the tropical Pacific. See the main texts and Table 2 for statistical details. Abbreviations in the legend box are labeled as follow: EQS, equatorial strip; ROD, rest of the domain.

larger PP_0 ($= 82.6\text{--}89.5 \text{ g C m}^{-2} \text{ yr}^{-1}$) than in the Atlantic, but k is much smaller ($k = 1.76 \pm 0.02 \times 10^{-4} \text{ m}^{-2}$), and hence the equatorial strip appears to be less efficiently productive for enhanced upwelling in this ocean. PP is nearly constant between $H = 275$ and 300 m. This largely occurs in the western tropical Pacific (see Fig. 3A). Here the rainfall is exceptionally heavy and so surface salinity is significantly reduced. This province is characterized by a shallow halocline not suitable for an algal bloom, constraining production. In the eastern equatorial Pacific, there is little iron, which is a biogeochemical constraint for production. As a result, the productivity curve corresponding to the eastern equatorial upwelling ($H < 270$ m) is much more gentle than that in the Atlantic case (Fig. 5A). Enhancement of upwelling does not strongly support primary production in the tropical Pacific.

Gao et al. (2000) showed that the whole Pacific has about half (46%) the amount of annual aeolian iron deposition of the whole Atlantic. Over the tropical Atlantic basin, the northeasterly and southeasterly trades transport massive amounts of dust that originate in the Sahara and Namib Deserts, respectively, throughout the year. In contrast, the climate of western South America might not be a sufficient iron source for the broad tropical Pacific. The southeasterly

trades in this ocean, therefore, provide little iron-rich dust to the eastern tropical Pacific.

The variance of the primary productivity through the Atlantic ROD is larger than in the Pacific ROD. The regression curves, based on Eq. 12, explain less than half the spatial variance of primary productivity in the upwelling regions (Table 2). Interestingly, the Atlantic ROD shows less explained variance than its Pacific counterpart: 36.0% and 46.2% for the Atlantic and Pacific, respectively. This suggests a complexity of mechanisms beyond climatological upwelling; at least, quantitative relationships between micronutrients to macronutrients, grazers, and upwelling need to be addressed. As an example of this, seasonal variability of iron deposition is much larger in the Atlantic than in the Pacific in both hemispheres (Gao et al. 2000). Hence there should be strong seasonal responses of the ocean to iron inputs, which cannot be explained by annual mean upwelling. In fact, when we separated ROD into two hemispheres, the southern hemisphere parts of both the tropical Atlantic and Pacific showed better fits of the model upwelling to primary productivity (Table 2). This emphasizes the strong seasonal variability of the possibly iron-limited ecosystem in the northern tropics and shows the limitation of the ocean model's evaluation of primary productivity. By contrast, in

the equatorial region the regression curves explain much of the spatial variance of primary productivity. This is very robust in the equatorial regime (EQS) of the Atlantic (84.2%).

f-ratio—We will briefly address the *f*-ratios for the downwelling, oligotrophic subtropical gyres and upwelling regions. Using the Redfield ratio between carbon and nitrogen (106:16), if the vertical gradient of mean nitrate and eddy-diffusion coefficient are given by $0.045 \mu\text{mol N L}^{-1} \text{m}^{-1}$ and $3.7 \times 10^{-5} \text{m}^2 \text{s}^{-1}$, respectively (Lewis et al. 1986), we evaluate $NP_0 = 4.17 \text{g C m}^{-2} \text{yr}^{-1}$. Using our estimates of PP_0 , *f*-ratios for the Atlantic and Pacific RODs are 0.05 and 0.06, respectively. These low values are typical of *f*-ratios in the subtropical gyres (Eppley and Peterson 1979) and are clearly distinguishable from the estimates of tropical upwelling regions (Chavez et al. 1996; Planas et al. 1999). For example, using a mean new production rate of $32.2 \text{g C m}^{-2} \text{yr}^{-1}$ in the equatorial Atlantic of 15°S – 15°N (Eppley and Peterson 1979) and the mean PP over this region from the VGPM ($138.5 \text{g C m}^{-2} \text{yr}^{-1}$), we estimate an *f*-ratio of 0.23. On the other hand, reconstructed PP through Eq. 12 and its corresponding new production through the curve of Berger et al. (1989), appropriate for that domain is $127.4 \text{g C m}^{-2} \text{yr}^{-1}$ and $34.5 \text{g C m}^{-2} \text{yr}^{-1}$, respectively. Hence our predicted tropical upwelling *f*-ratio is 0.27, which is in good agreement with the value of Eppley and Peterson (1979). It is, therefore, suggested that Eq. 12 is capable of examining basin-scale *f*-ratios.

Discussion and conclusions: Toward palaeocean modeling

Climatological upwelling and downwelling has been predicted by the reduced-gravity model. In this paper we used the model upper layer thickness as a proxy for upwelling and compared it with remotely sensed primary productivity estimated by Behrenfeld and Falkowski (1997a,b). This is the first report to validate the upwelling of the reduced-gravity model against remotely sensed productivity at basin scale. A simple relationship between the upper layer thickness and primary productivity is proved to be useful. It is worth noting that Eq. 12 explains much of the variance in primary productivity in the equatorial regimes (Table 2). In the light of the nutrient balance of the nitraclinic upper ocean, the eutrophic upwelling and oligotrophic downwelling zones are clearly separated by the *f*-ratio derived by Eq. 12. This implies that reduced-gravity modeling can provide a quantitative method for estimating tropical primary productivity.

We have shown that there is a difference in the upwelling–productivity relationship between the Atlantic and Pacific. The Atlantic appears to have more efficient production corresponding to the same degree of wind-driven upwelling than the Pacific, which is best featured in the equatorial region. This is ascribed to two major causes: (1) a low salinity unsuitable for algal blooms in the western tropical Pacific (Lukas and Lindstrom 1991), and (2) little aeolian iron input over the eastern equatorial Pacific (Longhurst 1998; Gao et

al. 2000). The zonal width of the Pacific basin amplifies these features. First, a convection centre is found over the western tropical Pacific oceanic continent, while the equivalent system in the Atlantic is over South America. This geographic constraint is responsible for heavier rainfall over the western tropical Pacific, sustaining the low salinity and shallow halocline. In the Atlantic, the bulk of the precipitation falls over the Amazonian Basin, and a significantly low salinity region is not found in the western tropical Atlantic, except near the mouth of the Amazon River. Second, regardless of the existence of deserts upstream of the trades, the broad tropical Pacific basin tends to have little aeolian iron supply, while plenty of aeolian iron from the Sahara and Namib deserts is provided to the narrow tropical Atlantic (see also Gao et al. 2000).

To conclude, we would like to link this study to reduced-gravity modeling in the late Quaternary (Luther et al. 1990) and the middle Cretaceous (Handoh et al. 1999). Palaeocean modeling studies must grapple with many unknown factors (Handoh 2001), and are sensitive to the results of palaeoclimate modeling that supply palaeocean modelers with wind fields of the geologic past. While there must be clear uncertainty in any wind field produced by such palaeoclimate models, the well-known palaeogeography will provide sufficient restriction to the palaeoclimate simulation for there to be some confidence in the large-scale features of the modeled marine atmosphere (Handoh et al. 1999). Here we have shown that climatological biological productivity through the tropics can be assessed by a reduced-gravity model forced by a climatological wind. This addresses the model's ability to predict where upwelling is strong enough for enhanced primary productivity, which is key to many palaeoceanographic studies (Parrish and Curtis 1982; Pedersen and Calvert 1990). For example, Handoh et al. (1999) have shown a direct link between palaeo-upwelling and black-shale deposits, the latter being potential petroleum source rocks. This analysis is now more convincing because of the quantitative link between model and productivity established in this paper. For palaeocean studies, our model result can be compared with independent quantitative sedimentary data (Handoh 2001). Regression analysis of these two independent estimates (as done here) will tell us about both the efficiency of palaeoproduction and the component of the palaeoproduction sustained by eddy diffusion of nutrient. This will shed new insights into the broad marine ecological background of the geologic past.

The ability to explore the location of palaeo-upwelling sites is linked with many economically important sedimentary deposits, such as phosphates, gas hydrates, and petroleum source rocks (Parrish and Curtis 1982; Handoh 2001). In combination with our past work (Handoh et al. 1999), we have here shown that palaeocean modeling could be a quantitatively reliable tool for successful prediction of such economically important sites. Of course, attention must be paid to the palaeogeographic distribution of aeolian iron (Janecek and Rea 1983) and micronutrients to macronutrients in the ocean. The proto-Atlantic was, however, even narrower than the modern-Atlantic, so that the model upwelling–productivity relationship is likely to have been robust into the past.

References

- BEHRENFELD, M. J., AND P. G. FALKOWSKI. 1997a. Photosynthetic rates derived from satellite-based chlorophyll concentration. *Limnol. Oceanogr.* **42**: 1–20.
- , AND ———. 1997b. A consumer's guide to phytoplankton primary productivity models. *Limnol. Oceanogr.* **42**: 1479–1491.
- , AND Z. C. KOLBER. 1999. Widespread iron limitation of phytoplankton in the South Pacific Ocean. *Science* **283**: 840–843.
- BERGER, W. H., V. S. SMETACEK, AND G. WEFER. 1989. Ocean productivity and paleoproductivity—An overview, p. 1–34. *In* W. H. Berger, V. S. Smetacek, and G. Wefer [eds.], *Productivity of the ocean: Present and past*. Wiley.
- BIGG, G. R., AND M. INOUE. 1992. Rossby waves and El Niño during 1935–46. *Q. J. R. Meteorol. Soc.* **118**: 125–152.
- BONILLA, J., W. J. BUGDEN, O. ZAFIRIOU, AND R. JONES. 1993. Seasonal distribution of nutrients and primary productivity on the eastern continental shelf of Venezuela as influenced by the Orinoco River. *J. Geophys. Res.* **98**: 2245–2257.
- BUSALACCHI, A. J., AND F. BLANC. 1989. On the role of closed and open boundaries in a model of the tropical Atlantic Ocean. *J. Phys. Oceanogr.* **19**: 831–841.
- CAMERLENGO, A. L., AND J. J. O'BRIEN. 1980. Open boundary conditions in rotating fluids. *J. Comput. Phys.* **35**: 12–35.
- CHAVEZ, F. P., K. R. BUCK, S. K. SERVICE, J. NEWTON, AND R. T. BARBER. 1996. Phytoplankton variability in the central and eastern tropical Pacific. *Deep-Sea Res.* **43**: 835–869.
- CULLEN, J. J., M. R. LEWIS, C. O. DAVIS, AND R. T. BARBER. 1992. Photosynthetic characteristics and estimated growth-rates indicate grazing is the proximate control of primary production in the equatorial Pacific. *J. Geophys. Res.* **97**: 639–654.
- EPPLEY, R. W., AND B. J. PETERSON. 1979. Particulate organic matter flux and planktonic new production in the deep ocean. *Nature* **282**: 677–680.
- GAO, Y., Y. J. KAUFMAN, D. TANRÉ, D. KOLBER, AND P. G. FALKOWSKI. 2000. Seasonal distributions of aeolian iron fluxes to the global ocean. *Geophys. Res. Lett.* **383**: 508–511.
- HANDOH, I. C. 2001. Oceanic upwelling through the evolution of the tropical Atlantic Basin, Ph.D. thesis. School of Environmental Sciences, University of East Anglia, Norwich, England.
- , G. R. BIGG, E. J. W. JONES, AND M. INOUE. 1999. An ocean modelling study of the Cenomanian Atlantic: Equatorial paleo-upwelling, organic-rich sediments and the consequences for a connection between the proto-North and South Atlantic. *Geophys. Res. Lett.* **26**: 223–226.
- HELLERMAN, S., AND M. ROSENSTEIN. 1983. Normal monthly wind stress over the world ocean with error-estimates. *J. Phys. Oceanogr.* **13**: 1093–1104.
- HERZFELD, U. C. 1992. Quantitative spatial models of Atlantic primary productivity—an application of geomathematics. *J. Geophys. Res.* **97**: 717–732.
- INOUE, M., AND J. J. O'BRIEN. 1986. Predictability of the decay of the 1982/83 El Niño. *Mon. Weather Rev.* **114**: 967–972.
- , AND S. WELSH. 1993. Modeling seasonal variability in the wind-driven upper-layer circulation in the Indo-Pacific region. *J. Phys. Oceanogr.* **23**: 1412–1436.
- JANECEK, T. R., AND D. K. REA. 1983. Eolian deposition in the northeast Pacific Ocean: Cenozoic history of atmospheric deposition. *Geol. Soc. Am. Bull.* **94**: 730–738.
- LEVITUS, S., AND T. P. BOYER. 1994. *The World Ocean Atlas 1994*. NOAA.
- LEWIS, M. R., W. G. HARRISON, N. S. OAKEY, D. HEBERT, AND T. PLATT. 1986. Vertical nitrate fluxes in the oligotrophic ocean. *Science* **234**: 870–873.
- LONGHURST, A. 1998. *Ecological geography of the sea*. Academic.
- , S. SATHYENDRANATH, T. PLATT, AND C. CAVERHILL. 1995. An estimate of global production in the ocean from satellite radiometer data. *J. Plankton Res.* **17**: 1245–1277.
- LUKAS, R., AND E. LINDSTROM. 1991. The mixed layer of the western equatorial Pacific Ocean. *J. Geophys. Res.* **96**: 3343–3357.
- LUTHER, M. E., J. J. O'BRIEN, AND W. L. PRELL. 1990. Variability in upwelling fields in the northwestern Indian ocean. I. Model experiments for the past 18,000 years. *Paleoceanography* **5**: 433–445.
- MCCREARY, J. P., AND P. K. KUNDU. 1988. A numerical investigation of the Somali Current during the Southwest Monsoon. *J. Mar. Res.* **46**: 25–58.
- MÜLLER-KARGER, F. E., C. R. MCCLAIN, AND P. L. RICHARDSON. 1988. The dispersal of the Amazon's water. *Nature* **333**: 56–59.
- NAVAL OCEANOGRAPHIC OFFICE. 1983. DBDB5 (Digital Bathymetric Data Base—5 minute grid). U.S.N.O.O.
- O'BRIEN, J. J., D. ADAMEC, AND D. W. MOORE. 1978. A simple model of upwelling in the Gulf of Guinea. *Geophys. Res. Lett.* **5**: 641–644.
- PARRISH, J. T., AND R. L. CURTIS. 1982. Atmospheric circulation, upwelling, and organic-rich rocks in the Mesozoic and Cenozoic eras. *Palaeogeogr. Palaeoclimatol. Palaeoecol.* **40**: 31–66.
- PEDERSEN, T. F., AND S. E. CALVERT. 1990. Anoxia vs. productivity: What controls the formation of organic-carbon-rich sediments and sedimentary rocks? *Am. Assoc. Pet. Geol. Bull.* **74**: 454–466.
- PLANAS, D., S. AGUSTI, C. M. DUARTE, T. C. GRANATA, AND M. MERINO. 1999. Nitrate uptake and diffusive nitrate supply in the Central Atlantic. *Limnol. Oceanogr.* **44**: 116–126.
- PRICE, N. M., B. A. AHNER, AND F. M. MOREL. 1994. The equatorial Pacific Ocean: Grazer-controlled phytoplankton populations in an iron-limited ecosystem. *Limnol. Oceanogr.* **39**: 520–534.
- UZ, B. M., J. A. YODER, AND V. OSYCHNY. 2001. Pumping nutrient to ocean surface waters by the action of propagating planetary waves. *Nature* **409**: 597–600.
- WUNSCH, C. 1984. An estimate of the upwelling rate in the equatorial Atlantic based on the distribution of bomb radiocarbon and quasi-geostrophic dynamics. *J. Geophys. Res.* **89**: 7971–7978.

Received: 16 November 2000

Accepted: 3 July 2001

Amended: 24 July 2001